Analytic RF design of a linear accelerator with a SLED-I type RF pulse compressor

Jia-Yang Liu[1,2] · **Jia-Ru Shi**[1,2] · **Hao Zha**[1,2] · **Alexej Grudiev**[3] ·
Ping Wang[1,2] · **Ying-Chao Du**[1,2] · **Huai-Bi Chen**[1,2]

Abstract This study presents the RF design of a linear accelerator (linac) operated in single-bunch mode. The accelerator is powered by a compressed RF pulse produced from a SLED-I type RF pulse compressor. The compressed RF pulse has an unflattened shape with a gradient distribution which varies over the structure cells. An analytical study to optimize the accelerating structure together with the RF pulse compressor is performed. The optimization aims to maximize the efficiency by minimizing the required RF power from the generator for a given average accelerating gradient. The study shows that, owing to the compressed RF pulse shape, the constant-impedance structure has a similar efficiency to the optimal structure using varying iris apertures. The constant-impedance structure is easily fabricated and is favorable for the design of a linac with a pulse compressor. We utilize these findings to optimize the RF design of a X-band linac using the constant-impedance accelerating structure for the Tsinghua Thomson X-ray source facility.

1 Introduction

Linear accelerators (linacs) have been investigated for many applications. The design of linear accelerators potentially benefits from the use of X-band high-gradient accelerating structures to shorten the accelerator design [1]. Normal-conducting X-band technologies have been developed for future lepton linear collider projects over the several past decades [2–4]. Recent experiments have demonstrated that a gradient of 100 MV/m is achievable for X-band structures with a radio frequency (RF) breakdown rate of less than 10^{-5}/pulse/m [5–7].

The power consumption is proportional to the square of the accelerating gradient. High-gradient accelerating structures consequently require more input power and increased investment in RF power sources. The RF pulse compressor alleviates the need for power source investments [8]. It converts the long pulse from the power generator to a short pulse with a higher power level. In several applications, such as the free electron laser (FEL) [9] and the Thomson scattering source [10], the linacs are operated in single-bunch mode and require a short pulse length. Therefore, the use of a RF pulse compressor is preferable in these single-bunch applications.

The present work is motivated by the design and optimization of such a X-band (11.424 GHz) linac with a SLED-I type pulse compressor. This X-band linac will be used in the injector of the Tsinghua Thomson scattering

✉ Hao Zha
zha_hao@mail.tsinghua.edu.cn

Jia-Yang Liu
liujiaya16@mails.tsinghua.edu.cn

1   Department of Engineering Physics, Tsinghua University, Beijing 100084, China

2   Key Laboratory of Particle and Radiation Imaging (Tsinghua University), Ministry of Education, Beijing 100084, China

3   European Organization for Nuclear Research (CERN), 1211 Geneva, Switzerland

X-ray (TTX) facility [11]. It will boost the electron beam from the current 50 meV to 150 meV, as shown in Fig. 1.

Given the space limitation in the bunker, the active length of this X-band structure should not be greater than 1.3 m, and a gradient of 80 MV/m is required. Such a X-band structure demands a RF input power greater than 120 MW. The RF pulse compressor has a power gain of more than 3, so a 50 MW X-band klystron suffices as the power supply. The RF pulse compressor used in this work was obtained from Ref.[12] and is a SLED-I type compressor with a compact and easily operated design. The compressed RF pulse shape is not flat, i.e., the power varies over time, as shown in Fig. 2. The facility is operated in single-bunch mode, and the electron bunch will be accelerated at the maximum voltage point in every RF pulse. However, the time-varying RF power travels through the structure at a limited speed (group velocity); thus, the upstream and downstream cells in the structure experience different input powers, thereby changing the distribution of the gradient. Detailed discussions will be presented in Sect. 2.

The geometry of the X-band structure is optimized in this work to minimize the RF power required from the generator. This optimization is important in the TTX facility for 2 reasons: the klystron is more stable at lower power levels, and the spare power can be used to operate other X-band devices such as a RF photocathode gun [13], a deflecting cavity [14, 15], or a linearizer [16]. Section 3 analytically explores the optimum solution for the accelerating structure. The study shows that the compressed RF pulse results in a near-optimum solution for the constant-impedance structure. The constant-impedance structure uses an identical structure geometry for each regular cell. It is more easily fabricated than the common traveling wave (TW) structure with varying iris apertures. The study in Sect. 3 demonstrates that a constant-impedance structure is favorable for the linac design if a SLED-I type RF pulse compressor is used. The concept of utilizing a constant-impedance structure as a near-optimum solution was also presented in Ref.[17].

We implemented this concept to develop the RF design of the X-band linac in the TTX facility, which uses a constant-impedance structure as the nominal accelerating
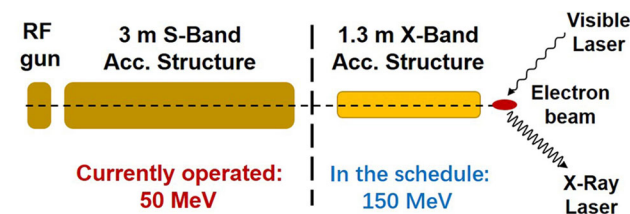

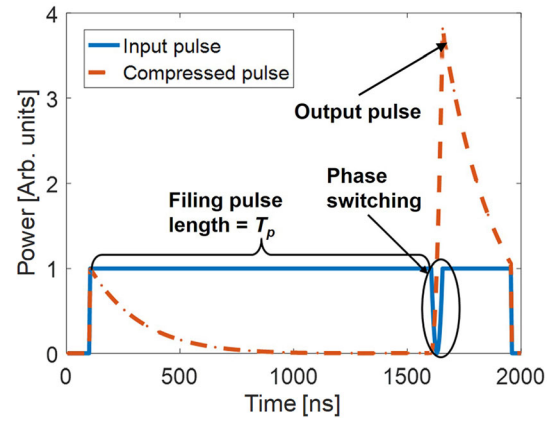**Fig. 1** Layout of TTX facility

Fig. 2 Schematic diagram of the RF pulse shape before and after the compressor

structure design. Another design using varying iris apertures is also discussed and compared with the nominal design. Further details will be presented in Sect. 4. The study in this work will be useful for designing linacs operated in single-bunch mode for other similar applications [18–20], such as X-band FEL sources [21–27] and Thomson sources [28]. In the two-beam acceleration scheme, the RF pulse generated by the drive beam delivered in single-bunch mode [29–32] has a shape similar to that produced by the SLED-I type RF pulse compressor. The discussion in this work is hence also helpful in studying two-beam acceleration.

2 Compressed RF pulse in the TW structure

The principle of the SLED-I type RF pulse compressor is described in Ref.[8]. The pulse shape of the compressed output RF power (dashed line in Fig. 2) can be expressed by the following formulas:

$$P(t) = P_0((A - \Gamma)\mathrm{e}^{-\mu t} + \Gamma)^2, \tag{1}$$

$$\mu = \omega \frac{1 + \beta}{2Q_s}, \tag{2}$$

$$\Gamma = \frac{1 - \beta}{1 + \beta}, \tag{3}$$

where t is the time from the peak power point, P_0 is the klystron input power, A is the field amplitude at the peak power point, ω is the angular frequency, and β and Q_s are the coupling and quality factors of the storage cavity, respectively. The power gain factor A^2 is determined by the shape of the filling pulse and the time of the phase switching (see Fig. 2). In the ideal case, where the filling pulse is rectangular-shaped with a length of T_p and the phase is switched instantaneously, A can be analytically expressed as:

$$A = \Gamma + \frac{2\beta}{1+\beta}(2 - e^{-\mu T_p}). \tag{4}$$

Figure 3a shows that the compressed RF power flows from the upstream cells to successive downstream cells in the X-band structure at a speed equal to the group velocity of the structure. The maximum accelerating voltage is achieved when the wave front of the peak RF power and the electron bunch arrive simultaneously at the end of structure, as shown in Fig. 3b.

The wall loss in the structure attenuates the RF power traveling within it. The RF power versus the longitudinal position z and the time t are expressed in the formulas below:

$$P(z, t) = P(0, t - T(z))e^{-\alpha(z)}, \tag{5}$$

$$T(z) = \int_0^z \frac{ds}{v_g}, \tag{6}$$

$$\alpha(z) = \int_0^z \frac{\omega}{Q v_g} ds, \tag{7}$$

where $T(z)$ is the filling time, $\alpha(z)$ is the attenuation factor, v_g is the group velocity, and Q is the quality factor. The detailed derivation of Eqs. (5–7) is shown in Refs.[33, 34]. Assuming that the electron bunch passes through the

structure at the speed of light, the gradient of each cell is expressed as:

$$G(z) = G\left(z, t_0 + \frac{z}{c}\right) = \sqrt{\omega \frac{R}{Q} \frac{P\left(z, t_0 + \frac{z}{c}\right)}{v_g}}, \tag{8}$$

where R is the shunt impedance per unit length and t_0 is the time point at which the beam enters the inlet of the structure.

To obtain the maximum voltage, the peak RF power and the electron bunch should arrive at the end of the structure simultaneously, such that

$$t_0 + \frac{L}{c} = T(L) = T_f, \tag{9}$$

where L is the length of one structure unit and T_f is the filling time. From Eqs. (1), (5), and (8), the gradient as a function of z can be given as:

$$\begin{aligned} G(z) &= \sqrt{\omega \frac{R}{Q} \frac{P\left(z, T(L) - \frac{L}{c} + \frac{z}{c}\right)}{v_g}} \\ &= \sqrt{\omega \frac{R}{Q} \frac{P\left(0, T(L) - T(z) - \frac{L}{c} + \frac{z}{c}\right)e^{-\alpha(z)}}{v_g}} \\ &= \sqrt{\omega \frac{R}{Q} \frac{P_0 e^{-\alpha(z)}}{v_g} F}, \end{aligned} \tag{10}$$

$$F = (A - \Gamma)e^{-\mu\left(T(L) - \frac{L}{c}\right) + \mu\left(T(z) - \frac{z}{c}\right)} + \Gamma, \tag{11}$$

where the coefficient F represents the gradient gain due to the RF pulse compressor. According to Eqs. (1) and (4), $A > \Gamma$; thus, F is an increasing function of z. Figure 4 shows an example of the gradient distribution with and without the RF pulse compressor.
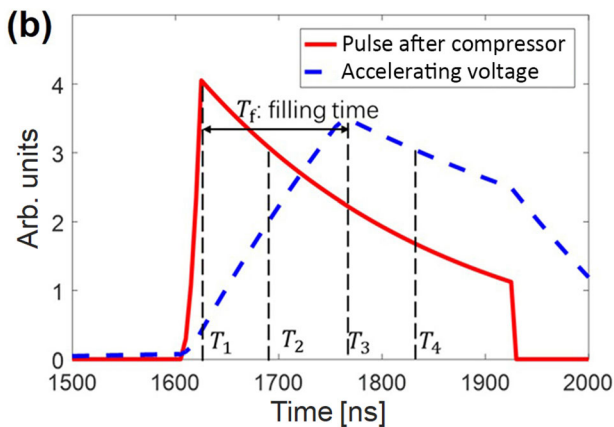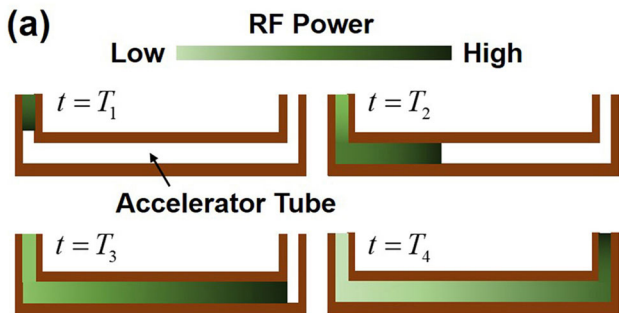

Fig. 3 **a** Power flow in the traveling wave structure at different times; **b** Accelerating voltage of the structure versus time
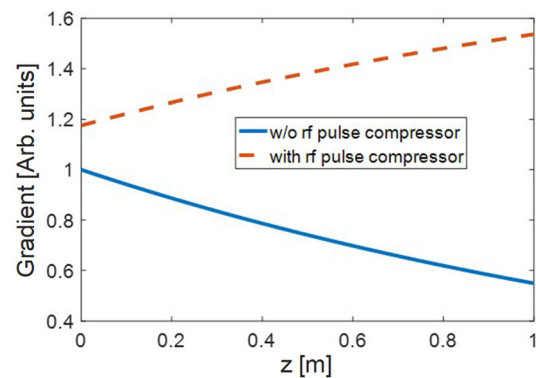

Fig. 4 Change of distribution gradient by the RF pulse compressor

3 Analytical optimization of the gradient distribution

This section explores the optimum solution that minimizes the input power for a given gradient. This optimization is equivalent to maximizing the effective shunt impedance R_{eff} of the whole system [17], which is defined by the ratio of the average gradient $\overline{G}$ and the required input power from the klystron:

$$R_{eff} = \frac{\overline{G}^2 L}{P_0}, \tag{12}$$

$$\overline{G} = \frac{1}{L} \int_0^L G(z) dz. \tag{13}$$

For large accelerator projects such as linear colliders, the AC power consumption is significant. Thus, the optimization of these applications should also consider additional parameters such as the RF pulse length and the beam current. The study in this work will focus on maximizing R_{eff} because the investment in the power sources is much more expensive than the electricity in our application.

Equation (8) indicates that the gradient is calculated from R, Q, and v_g. Traveling wave accelerating structures usually have iris apertures that are tapered from the upstream cells to the downstream cells. The tapering results in the variation of v_g from cell to cell, but the variations of R and Q are insignificant compared to that of v_g. R and Q are assumed to be constant functions of z in this section. In this case, the distribution of the gradient is determined by $v_g = v_g(z)$, which needs to be solved in the design work of the accelerating structure. If a RF pulse compressor is not used (F in Eq. (10) is 1), the integral of the square of the gradient can be written in a simple form:

$$\|G(z)\|^2 = \frac{1}{L} \int_0^L G^2(z) dz = \int_0^L \frac{P_0 R\omega}{LQv_g} e^{-\alpha(z)} dz$$
$$= \int_0^L \frac{P_0}{L} R e^{-\alpha(z)} d\alpha(z) = \frac{P_0}{L} R \left(1 - e^{-\alpha(L)}\right), \tag{14}$$

From Eqs. (6) and (7), $\alpha(L)$ is equal to $\omega T_f/Q$. For a given P_0, R, and T_f, the right side of Eq. (14) has a constant value regardless of the form of $v_g(z)$. In the calculus of variations, $G(z)$ is an element or vector in a Banach space. Equation (14) provides the Euclidean norm of $G(z)$. According to the Cauchy–Schwarz inequality $\overline{G} = \langle G(z), 1 \rangle \leq \|G(z)\|\|1\| = \|G(z)\|$. From Eqs. (12) and (14), we have

$$R_{eff} = \frac{\overline{G}^2 L}{P_0} \leq \frac{\|G(z)\|^2 L}{P_0} = R\left(1 - e^{-\frac{\omega}{Q}Tf}\right). \tag{15}$$

The two sides of Eq. 15 are equal when $G(z)$ is equal to 1, which means that R_{eff} reaches its maximum when $G(z)$ is

a constant function. This indicates that the optimum solution is a constant-gradient structure. From Eq. (14), $e^{-\alpha(z)}$ should be a linear function of z. The form of $v_g(z)$ is given by the following equation, which is also a linear function of z:

$$v_g(z) = \frac{\omega}{Q \frac{d\alpha(z)}{dz}} = \frac{\omega}{Q} \left(\frac{L}{1 - e^{-\frac{\omega}{Q}T_f}} - z\right), \tag{16}$$

If the RF pulse compressor is used, then Eq. (15) can be rewritten as:

$$R_{eff} \leq \frac{\|G(z)\|^2 L}{P_0} = \int_0^L \frac{R\omega}{Qv_g} e^{-\alpha(z)} F^2(z) dz$$
$$= R\frac{\omega}{Q} \int_0^{T_f} e^{-\frac{\omega}{Q}T(z)} F^2(T(z)) dT(z), \tag{17}$$

where another assumption was made that the group velocity is much slower than the speed of light, i.e., $T(z) = z/v_g \gg z/c$; thus, the z/c and L/c terms in Eq. (10) can be ignored. Equation (17) indicates that if the filling time T_f is fixed, then the Euclidean norm of $G(z)$ does not depend on the specific form of $v_g(z)$. Therefore, the conclusion remains that the optimum solution is a uniformly distributed gradient when a RF pulse compressor is used. With a constant function as the gradient, v_g can be solved as a function of the filling time $T(z)$ based on Eq. (10):

$$v_g(T(z)) = \frac{\omega RP_0 e^{-\frac{\omega}{Q}T(z)}}{QG^2} F^2(T(z)). \tag{18}$$

One additional term F is included in the equation. It represents the effect of the pulse compressor on the solution of v_g. F is an increasing function of $T(z)$ such that the optimum solution of v_g decreases more slowly than the solution without the RF pulse compressor. Figure 5 shows the solutions of v_g with different parameters of the RF pulse compressor as examples. For a number of parameter
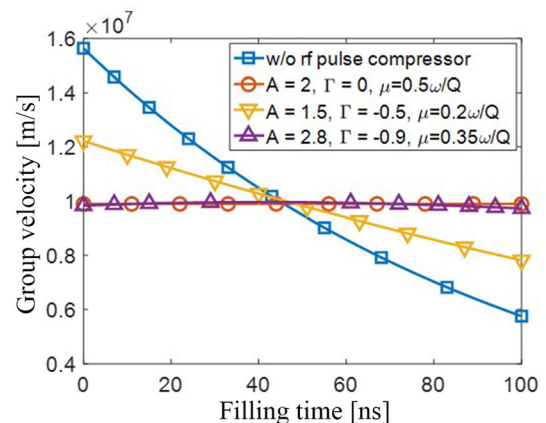

Fig. 5 (Color online) Optimum solution of group velocity v_g versus the filling time $T(z)$

sets, the solutions of v_g approximate constant functions, as shown in the second and fourth curves in Fig. 5. The constant v_g allows all the structure cells to use identical geometries, which is called the constant-impedance structure. Compared to a structure using linearly tapering iris apertures, the constant-impedance structure is significantly easier to fabricate and reduces the total cost of the accelerator.

However, the constant v_g solution requires particular parameters of the RF pulse compressor that are inconsistent with the global optimum for maximizing R_{eff}. The upper limit of R_{eff} given by Eq. (17) can be written as:

$$\text{Max}(R_{eff}) = R \int_0^{\tau_f} e^{-\tau} F^2(\tau) d\tau, \tag{19}$$

where

$$\tau = \frac{\omega}{Q} T(z),$$

$$F(\tau) = (A - \Gamma) e^{-\mu(T_f - \tau)} + \Gamma = \frac{2\beta}{1+\beta} \left(2 - e^{-\frac{Q(1+\beta)}{2Q_s} \tau_p} \right)$$

$$e^{-\frac{Q(1+\beta)}{2Q_s}(\tau_f - \tau)} + \frac{1-\beta}{1+\beta},$$

$$\tau_f = \frac{\omega}{Q} T_f$$

$$\tau_p = \frac{\omega}{Q} T_p. \tag{20}$$

From Eqs. (10), (12), and (13), the effective shunt impedance of the constant-impedance structure is written as:

$$R_{eff}^* = \frac{R\omega}{QL} \left(\int_0^L \frac{e^{-\frac{\omega z}{2Qv_g}}}{\sqrt{v_g}} F(z) dz \right)^2 = \frac{R}{\tau_f} \left(\int_0^{\tau_f} e^{-\frac{\tau}{2}} F(\tau) d\tau \right)^2. \tag{21}$$

The expressions of $\text{Max}(R_{eff})$ and R_{eff}^* contain 4 parameters: τ_f, β, Q/Q_s, and τ_p. All 4 parameters are dimensionless parameters, so the discussion here applies for all RF frequencies. The parameter Q/Q_s is the ratio of the quality factors in the regular accelerating cavities and the storage cavity of the pulse compressor, and τ_p represents the length of the filling pulse. These 2 parameters are usually given as numbers. The other 2 parameters τ_f and β can be optimized for the given τ_p and Q/Q_s. Figure 6 plots 2 effective shunt impedances for different τ_p and Q/Q_s with the optimum τ_f and β in each case. The discrepancy between $\text{Max}(R_{eff})$ and R_{eff}^* is less than 1%, which indicates that the constant-impedance structure performs similarly to the global optimum solution. The optimum τ_f and β that maximize the effective shunt impedance R_{eff}^* of the constant-impedance structure shown in Fig. 6b when the RF pulse compressor is used is presented in Fig. 7.
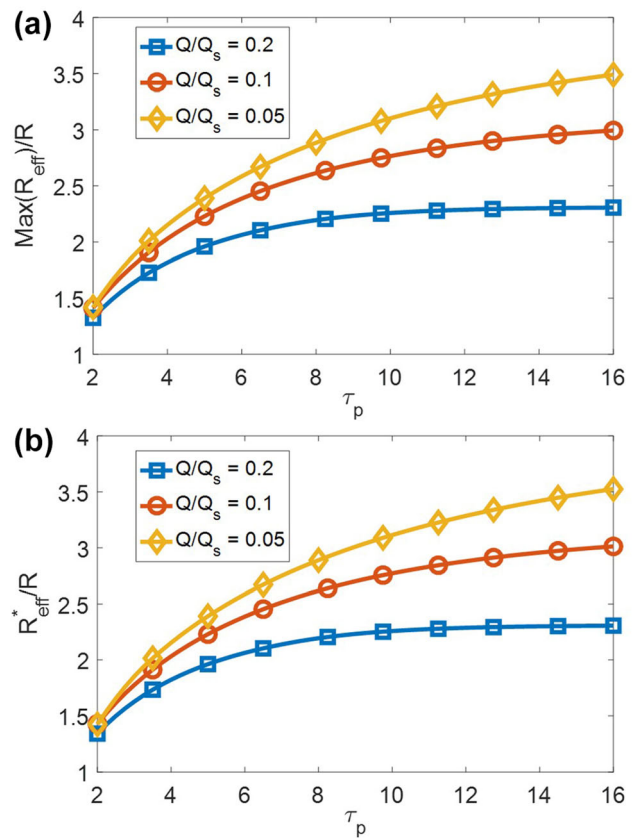

Fig. 6 (Color online) **a** $\text{Max}(R_{eff})$ and **b** R_{eff}^* versus τ_p and Q/Q_s at the optimum τ_f and β

If the RF pulse compressor is not used, $F(\tau)$ in Eqs. (19) and (21) is 1. In this case, the maximum R_{eff}^* for the constant-impedance structure is $0.81R$ when $\tau_f = 2.51$. The effective shunt impedance $\text{Max}(R_{eff})$ for the constant-gradient structure approximates R if τ_f is sufficiently large, as shown in Fig. 8. Note that a larger τ_f results in a longer filling time, which reduces the efficiency from the AC power to the beam. This calculation proves that the RF pulse compressor further optimizes the constant-impedance structure.

4 RF design of X-band linac for TTX facility

Section 3 analytically explored the optimum RF design of a traveling wave accelerating structure. The analysis was performed with the assumption that R and Q are constant values for all the cells in the structure. However, this assumption leads to inaccuracies if the structure cells have differing geometries. In this section, the RF parameters for 2 designs, namely the optimized constant-impedance structure and the optimized structure using varying iris apertures, are numerically calculated.
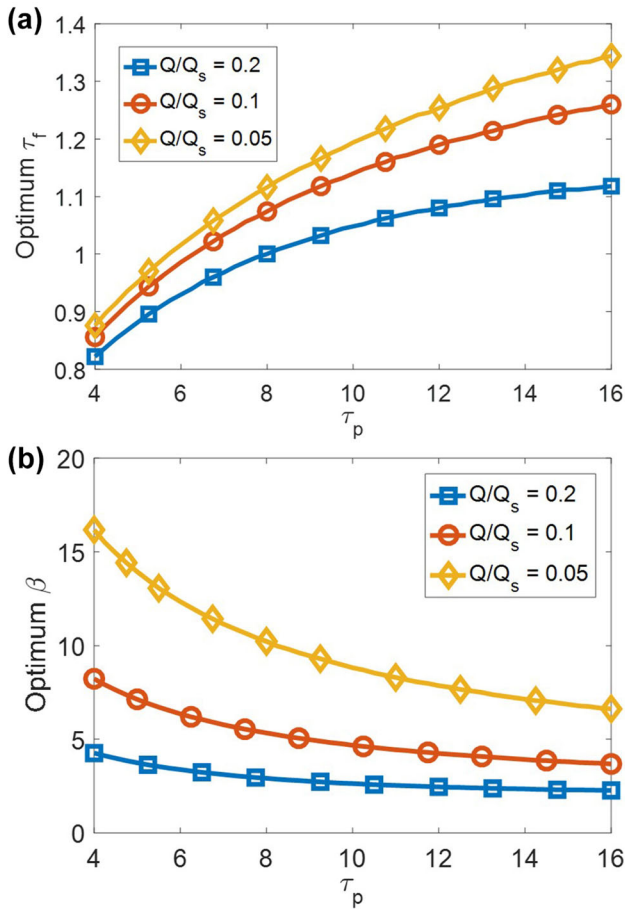
(a)

(b)

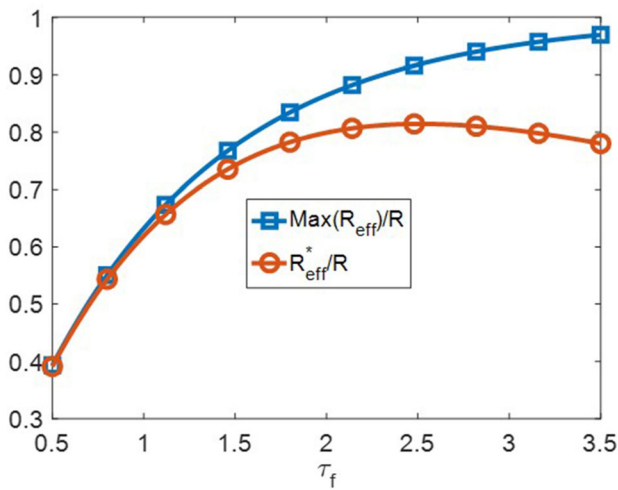**Fig. 7** Optimum **a** τ_f and **b** β for different τ_p and Q/Q_s

Fig. 8 Max(R_{eff}) and R_{eff}^* versus τ_f without RF pulse compressor

The cut view of a traveling wave accelerating structure cell is shown in Fig. 9. The phase advancement per structure cell is $2\pi/3$. The study of short-range wakefields requires the average radius of the iris aperture to not be less than 3.5 mm and the minimum radius to be larger than
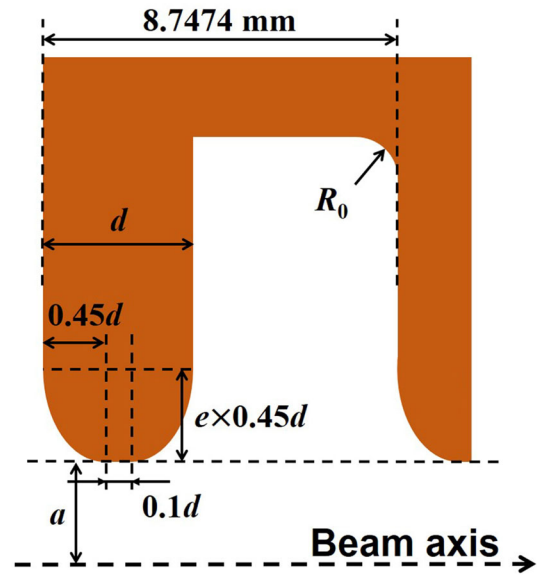

Fig. 9 Geometric sketch of a single cell

3 mm [35, 36]. With this aperture, the average group velocity is approximately 2.3% of the speed of light, and the quality factor Q is approximately 7200. The parameters of the RF pulse compressor in this work are similar to those in Refs.[12, 44]. The quality factor of the storage cavity Q_s is approximately 100,000. The total pulse length is approximately 1.5 μs; thus, τ_p is less than 14. According to Fig. 7a, the optimum τ_f is approximately 1.2, and thus the optimum filling time is given by $T_f = \tau_f Q/\omega = 120$ ns. The optimum active length of the structure is calculated as $v_g \times T_f \approx 0.8$ m. The required total active length of the X-band structure for the TTX facility is 1.3 m. The structure is hence divided into 2 identical structure units. Each structure unit has 72 structure cells and an active length of 0.63 m. Under these conditions, the optimum T_f is approximately 95 ns, and the optimum τ_f is approximately 1. These optimum parameters facilitate the RF design of the linac.

In actual operation, the phase switching takes time. This results in the factor A becoming less than the value obtained through the theoretical calculation in Eq. (4). This effect is not considered in this work because it complicates the estimation. The actual required power should be scaled by a factor that considers the phase switching effect as well as the losses in the power transmission system.

The nominal RF design of the linac for TTX uses a constant-impedance structure. The design has three parameters for investigation: the iris thickness d, the ratio of the major radius to the minor radius in the elliptical iris e, and the coupling factor of the pulse compressor storage cavity β. Here, the radius of the iris aperture a is 3.5 mm, and the rounding in the wall R_0 is 2.5 mm. We calculated

the RF parameters R, Q, and v_g of a single cell using the CST code [37]. The total required input power for the 2 structural units was calculated using Eq. (10) for average gradients of 80 MV/m.

Figure 10 plots the RF parameters of the structure versus β. The RF parameters include the required input power from the klystron, the maximum surface electric field E_s, and the maximum modified Poynting vector S_c [38] in the structure. The maximum surface fields were calculated from the gradient when the peak of the compressed power propagates in the cell. Figure 10a shows that β for the minimum input power is 5. A larger value of β, however, induces a larger power flow in the upstream of the structure, which consequently increases the maximum surface field E_s, and thus, S_c. According to a study on high-power tests of X-band accelerating structures, the RF breakdown rate is lower than 10^{-5}/pulse/m when the structure operates at a pulse length of 100 ns, $E_s < 200$ MV/m, and $S_{c-} < 5$ MW/mm^2 [7, 39]. Finally, β was set to 3.5 considering both the input power and the maximum surface fields. Figure 11 shows the RF parameters versus d and e. The optimum solution is $d = 1.8$ mm and $e = 1.3$ for the minimum input power under the condition that the maximum
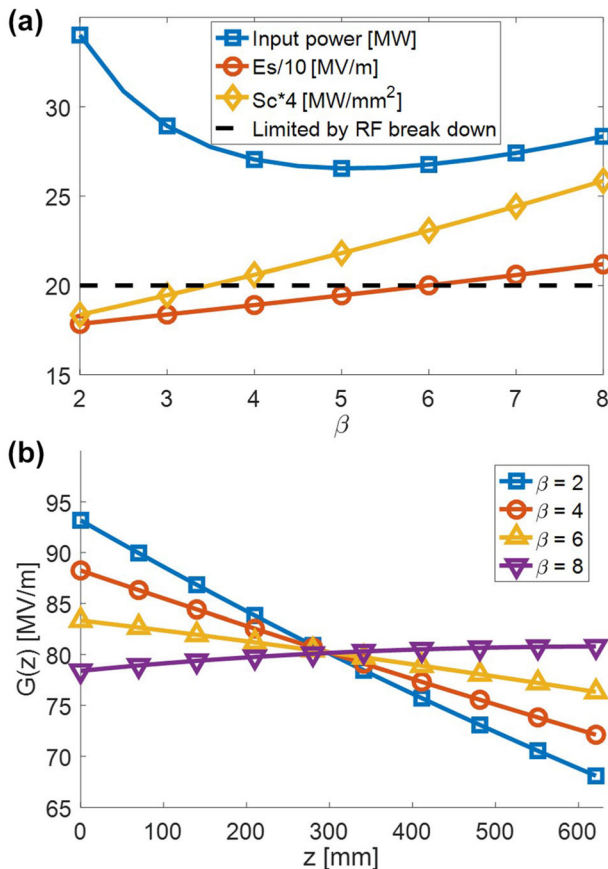
(a)

(b)

Fig. 10 (Color online) **a** RF parameters versus β; **b** Distribution of gradient seen by beam for different β
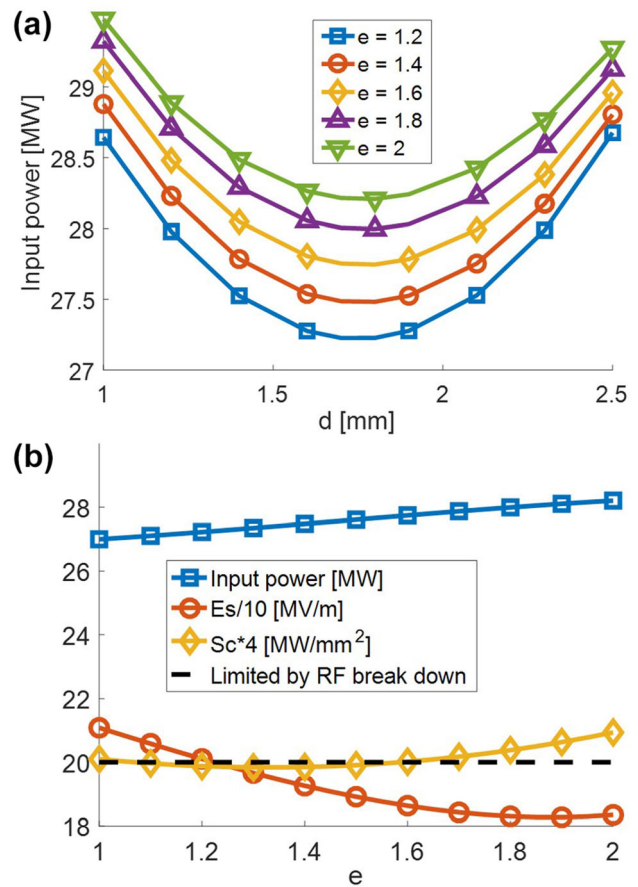
(a)

(b)

Fig. 11 (Color online) **a** Input power versus d and e; **b** RF parameters versus e

surface fields are below the limit set by the RF breakdown rate. The distributions of the normalized fields in the optimized single cell are shown in Fig. 12.

Another structure design with varying iris apertures, which often uses linear tapering on the iris apertures, is also discussed here. In this setup, the upstream cells have a large aperture such that the group velocity of these cells is higher than the average. This will reduce the gradient in the upstream cells to decrease the maximum surface fields in the structure. The strategy in this structure design uses the optimum value of $\beta = 5$ to minimize the input power, as shown in Fig. 13a. Figure 13b shows the maximum surface fields versus the tapering parameter Δa, which is the difference between the aperture radii of the first and the last cells. The optimum Δa for the minimum input power is 0.2 mm, and this Δa also has a flat gradient distribution as shown in Fig. 14, in agreement with the analytical results in Sect. 3. However, a Δa of 0.8 mm was finally selected to satisfy the criteria of the maximum surface fields. The optimization of d and e is similar to that of the constant-impedance structure design.

The final parameters of this structure are listed in Table 1 along with the parameters of the constant-

Fig. 12 (Color online) The distributions of normalized **a** electric field and **b** modified Poynting vector in the single cell
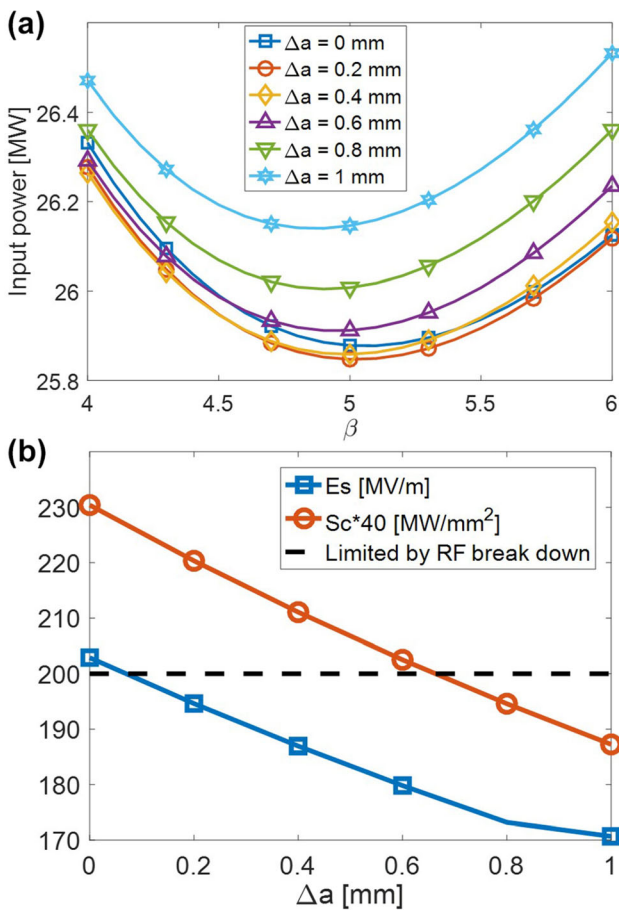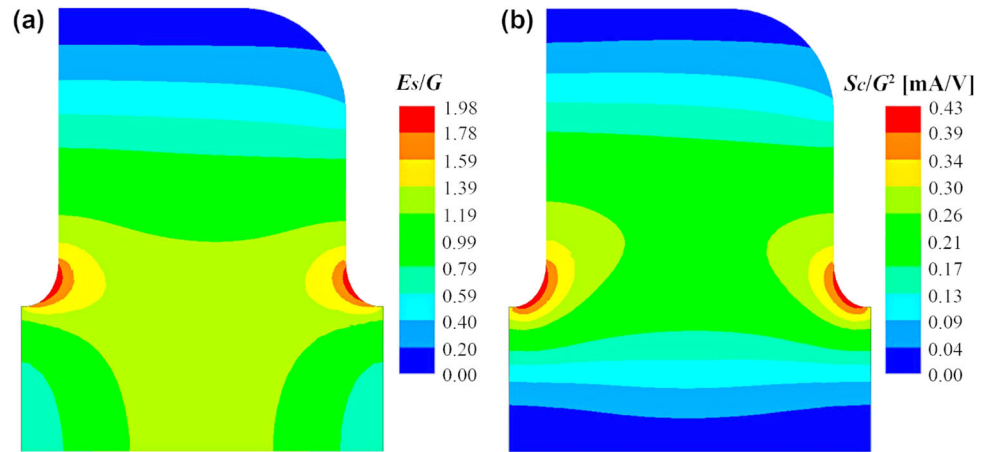

Fig. 13 (Color online) **a** Input power versus β and Δa; **b** Maximum surface fields versus Δa

Fig. 14 (Color online) Distribution of gradient seen by beam for different Δa

value of β for the nominal design is not optimal with respect to the maximum surface fields.

The final design of the constant-impedance structure has a total length of 0.7 m, as shown in Fig. 15. This structure is named as "TTX-XC72". The input and output couplers are both well matched to the WR90 waveguides with reflections of below −45 dB. The electric field along the beam path is simulated in CST [37] and shown in Fig. 16. The RF design of the SLED-I type RF pulse compressor using a corrugated circular cavity with a coupling coefficient of 3.5 has also been completed, as reported in Ref.[44]. The distribution of the field parameters in the accelerating structure operating with the compressed pulse is calculated analytically based on the parameters Q, R, v_g, and β listed in Table 1 and presented in Fig. 17.

The modulation of the output pulse shape of the SLED-I pulse compressor to reduce the peak output power for lower surface fields while retaining the same average output power (the gradient is the same) will be considered in future studies. Two ways of modulating the output pulse shape using correction cavities [40–42] or the phase

impedance structure. Both designs satisfy the criteria of maximum surface fields with a low breakdown rate. The tapering iris aperture design has a slightly lower input power than that of the nominal design using a constant-impedance structure. This phenomenon occurs because the
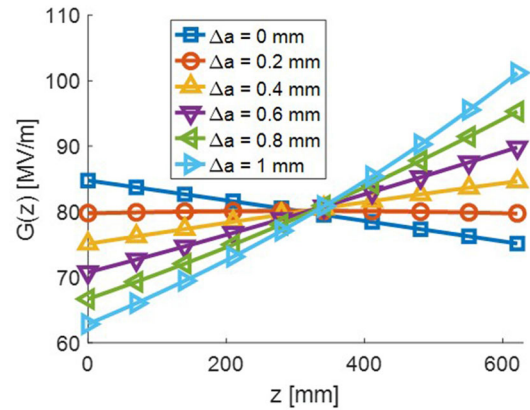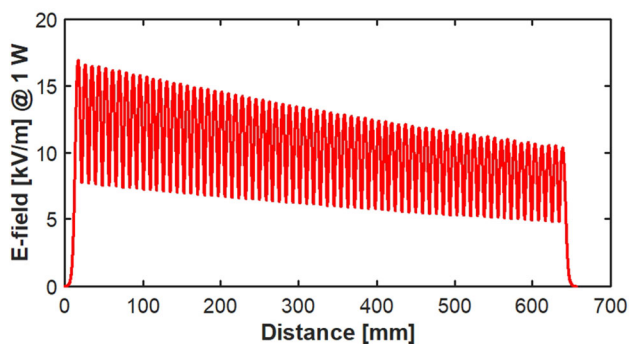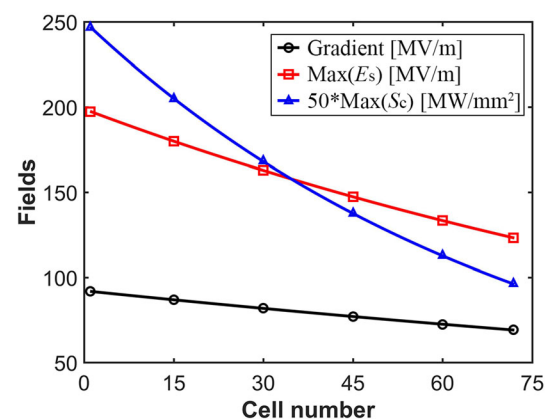
Table 1 RF parameters of two designs

	Tapering on iris aperture	Constant-impedance structure
Iris aperture a (mm)	3.92–3.12	3.5
Iris thickness d (mm)	1.7	1.8
Iris elliptical ratio e	1.0	1.3
Shunt impedance R (MΩ/m)	97–113	103
Group velocity v_g/c	3.33–1.47%	2.24%
Quality factor Q	7260–7200	7180
Filling time T_f (ns)	95	94
E_s (MV/m)	183	196
S_c (MW/mm^2)	4.57	4.96
β	5	3.5
Effective shunt impedance (MΩ/m)	311	295
Input power from klystron (MW)	25.9	27.3
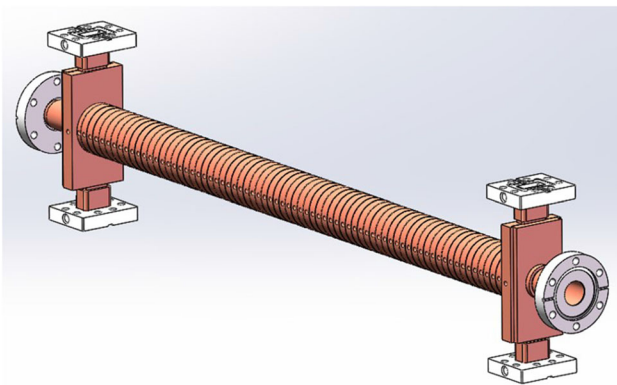
Fig. 15 Assembly of the constant-impedance accelerating structure for the TTX facility

Fig. 17 Distribution of field parameters for 80 MV/m gradient along the structure under the compressed pulse

Fig. 16 Magnitude of electric field along the beam path at 1 W input power

modulating SLED mode [43] will be studied for this application.

In conclusion, the constant-impedance structure design with its advantage of much easier fabrication is preferable for upgrades of the TTX facility. A structure prototype based on this constant-impedance structure design will be manufactured and tested in the near future.

5 Conclusion

The RF design of a X-band linac for the TTX source facility was discussed in this work. The linac was designed to boost the energy of the electron beam in the TTX facility from 50 to 150 meV. A SLED-I type RF pulse compressor is used to increase the obtained peak power such that a single 50 MW X-band klystron can support the operation of this structure at a gradient of 80 MV/m. The compressed RF pulse has an unflattened pulse shape, which changes the gradient distribution along the structure cells. The study showed that the gradients in the downstream cells increase more significantly than the gradients in the upstream cells.

The structure was optimized with the aim of reducing the required input power from the power source, so that the power source can operate more stably and provide spare power to feed other X-band devices. The analytical work proved that the optimum solution is a uniform distribution of the accelerating gradient. If the input RF pulse is flat, then the optimum solution is a constant-gradient structure. However, because the SLED-I type RF pulse compressor

changes the RF shape, the constant-impedance structure is a near-optimum solution.

Two designs, a nominal design using the constant-impedance structure and a structure with varying iris apertures, were optimized in this work. Both designs have similar input power requirements and satisfy the criteria of generating the maximum surface field at a low breakdown rate. The constant-impedance structure design is more easily fabricated and therefore favorable for the X-band linac of the TTX facility.

References

1. T. Higo, Y. Higashi, S. Matsumoto, et al., Advances in X-band TW accelerator structures operating in the 100 MV/m regime, in Proc. 1st Int. Particle Accelerator Conf. (IPAC'10), Kyoto, Japan, paper THPEA013, pp. 3702–3704 May (2010)
2. S. Doebert, C. Adolphsen, G. Bowden, et al., high gradient performance of NLC/GLC X-band accelerating structures, in Proc. 21st Particle Accelerator Conf. (PAC'05), Knoxville, TN, USA, paper ROAC004, pp. 372–374 May (2005)
3. H. Zha, A. Grudiev, Design and optimization of compact linear collider main linac accelerating structure. Phys. Rev. Accel. Beams 19, 111003 (2016). https://doi.org/10.1103/PhysRevAccelBeams.19.111003
4. G. Gatti, A. Marcelli, B. Spataro et al., X-band accelerator structures: on going R&D at the INFN. Nucl. Instrum. Method A. 829, 206–212 (2016). https://doi.org/10.1016/j.nima.2016.02.061
5. J. Wang, Research of RF high gradient physics and its application in accelerator structure development. High Gr. Accel. Struct. (2014). https://doi.org/10.1142/9789814602105_0002
6. A. Degiovanni, W. Wuensch, J. Navarro, Comparison of the conditioning of high gradient accelerating structures. Phys. Rev. Accel. Beams 19, 032001 (2016). https://doi.org/10.1103/PhysRevAccelBeams.19.032001
7. W. Wuensch, A. Degiovanni, S. Calatroni et al., Statistics of vacuum breakdown in the high-gradient and low-rate regime. Phys. Rev. Accel. Beams 20, 011007 (2017). https://doi.org/10.1103/PhysRevAccelBeams.20.011007
8. Z. D. Farkas, H. A. Hogg, G. A. Loew, et al., SLED: a method of doubling SLAC's energy, in Proc. 9th International Conference on High Energy Accelerators, Stanford, California, 2–7, pp. 576–583 May (1974)
9. C. Bostedt, S. Boutet, D.M. Fritz et al., Linac coherent light source: the first five years. Rev. Mod. Phys. 88, 015007 (2016). https://doi.org/10.1103/RevModPhys.88.015007
10. I.A. Artyukov, E.G. Bessonov, M.V. Gorbunkov et al., Thomson linac-based X-ray generator: a primer for theory and design. Laser. Part. Beams 34(4), 637–644 (2016). https://doi.org/10.1017/S0263034616000586
11. Y. Du, L. Yan, J. Hua et al., Generation of first hard X-ray pulse at tsinghua thomson scattering X-ray source. Rev. Sci. Instrum. 84, 053301 (2013). https://doi.org/10.1063/1.4803671
12. M. Franzi, J. Wang, V. Dolgashev et al., Compact rf polarizer and its application to pulse compression systems. Phys. Rev. Accel. Beams 19, 062002 (2016). https://doi.org/10.1103/PhysRevAccelBeams.19.062002
13. C. Limborg-Deprey, C. Adolphsen, D. McCormick et al., Performance of a first generation X-band photoelectron rf gun. Phys.
14. V.A. Dolgashev, G. Bowden, Y. Ding et al., Design and application of multimegawatt X-band deflectors for femtosecond electron beam diagnostics. Phys. Rev. ST Accel. Beams 17, 102801 (2014). https://doi.org/10.1103/PhysRevSTAB.17.102801
15. J. Tan, Q. Gu, W. Fang, et al., X-band deflecting cavity design for ultra-short bunch length measurement of SXFEL at SINAP. Nucl. Sci. Tech. 25, 060101 (2014). https://doi.org/10.13538/j.1001-8042/nst.25.060101
16. Y. Sun, P. Emma, T. Raubenheimer et al., X-band rf driven free electron laser driver with optics linearization. Phys. Rev. ST Accel. Beams 17, 110703 (2014). https://doi.org/10.1103/PhysRevSTAB.17.110703
17. A. Grudiev, Optimisation of single bunch linac for FERMI upgrade, in 7th annual workshop on high gradients (HG2013), https://indico.cern.ch/event/231116/contributions/1542978/attachments/383415/533338/Optimisation_of_single_bunch_linac_for_FERMI_upgrade_AG.pdf
18. F. Wang, C. Adolphsen, Normal conducting linac designs for low beam loading. Nucl. Instrum. Method A. 729, 605–614 (2013). https://doi.org/10.1016/j.nima.2013.08.013
19. M. Uesaka, K. Tauchi, T. Kozawa et al., Generation of a subpicosecond relativistic electron single bunch at the S-band linear accelerator. Phys. Rev. E 50, 3068 (1994). https://doi.org/10.1103/PhysRevE.50.3068
20. D. Alesini, M. Bellaveglia, M.E. Biagini et al., Design, realization and test of C-band accelerating structures for the SPARC_LAB linac energy upgrade. Nucl. Instrum. Method A. 837, 161–170 (2016). https://doi.org/10.1016/j.nima.2016.09.010
21. M. Schaer, A. Citterio, P. Craievich et al., rf traveling-wave electron gun for photoinjectors. Phys. Rev. Accel. Beams 19, 072001 (2016). https://doi.org/10.1103/PhysRevAccelBeams.19.072001
22. T. Inagaki, C. Kondo, H. Maesaka et al., High-gradient C-band linac for a compact x-ray free-electron laser facility. Phys. Rev. ST Accel. Beams 17, 080702 (2014). https://doi.org/10.1103/PhysRevSTAB.17.080702
23. W. Fang, Q. Gu, X. Sheng et al., Design, fabrication and first beam tests of the C-band RF acceleration unit at SINAP. Nucl. Instrum. Method A. 823, 91–97 (2016). https://doi.org/10.1016/j.nima.2016.03.101
24. W. Fang, Q. Gu, D. Tong et al., Design optimization of a C-band traveling-wave accelerating structure for a compact X-ray free electron laser facility. Chin. Sci. Bull. 56, 3420–3425 (2011). https://doi.org/10.1007/s11434-011-4754-y
25. Y. Joo, Y. Park, H. Heo et al., Development of new S-band SLED for PAL-XFEL linac. Nucl. Instrum. Method A 843, 50–60 (2017). https://doi.org/10.1016/j.nima.2016.11.005
26. G. D'Auria, X-band technology applications at FERMI@Elettra FEL project. Nucl. Instrum. Method A. 657, 150–155 (2011). https://doi.org/10.1016/j.nima.2011.06.048
27. A.A. Aksoy, Ö. Yavaş, E. Adli, et al., FEL proposal based on CLIC X-band structure, in Proc. 36th Int. Free Electron Laser Conf. (FEL'14), Basel, Switzerland, paper MOP062, pp. 186–189. Aug. (2014)
28. A. Bacci, D. Alesini, P. Antici et al., Electron linac design to drive bright Compton back-scattering gamma-ray sources. J. Appl. Phys. 113, 194508 (2013). https://doi.org/10.1063/1.4805071
29. M.D. Forno, V. Dolgashev, G. Bowden et al., rf breakdown tests of mm-wave metallic accelerating structures. Phys. Rev. Accel. Beams 19, 011301 (2016). https://doi.org/10.1103/PhysRevAccelBeams.19.011301

30. S.Y. Kazakov, S.V. Kuzikov, Y. Jiang et al., High-gradient two-beam accelerator structure. Phys. Rev. ST Accel. Beams **13**, 071303 (2010). https://doi.org/10.1103/PhysRevSTAB.13.071303

31. D. Wang, S. Antipov, C. Jing et al., Interaction of an ultrarelativistic electron bunch train with a W-band accelerating structure: high power and high gradient. Phys. Rev. Lett. **116**, 054801 (2016). https://doi.org/10.1103/PhysRevLett.116.054801

32. N.R. Neveu, M. Conde, D.S. Doran, et al., Drive generation and propagation studies for the two beam acceleration experiment at the argonne wakefield accelerator. in Proc. 7th Int. Particle Accelerator Conf. (IPAC'16), Busan, Korea, paper TUPMY036, pp. 1629–1631. May (2016)

33. A. Lunin, V. Yakovlev, A. Grudiev, Analytical solutions for transient and steady state beam loading in arbitrary traveling wave accelerating structures. Phys. Rev. ST Accel. Beams **14**, 052001 (2011). https://doi.org/10.1103/PhysRevSTAB.14.052001

34. O. Kononenko, A. Grudiev, Transient beam-loading model and compensation in compact linear collider main linac. Phys. Rev. ST Accel. Beams **14**, 111001 (2011). https://doi.org/10.1103/PhysRevSTAB.14.111001

35. A. Grudiev, Very short-range wakefields in strongly tapered disk-loaded waveguide structures. Phys. Rev. ST Accel. Beams **15**, 121001 (2012). https://doi.org/10.1103/PhysRevSTAB.15.121001

36. Wencheng Fang and Daniel Schulte, private communications.

37. CST https://www.cst.com

38. A. Grudiev, S. Calatroni, W. Wuensch, New local field quantity describing the high gradient limit of accelerating structures. Phys. Rev. ST Accel. Beams **12**, 102001 (2009). https://doi.org/10.1103/PhysRevSTAB.12.102001

39. F. Wang, C. Adolphsen, C. Nantista, Performance limiting effects in X-band accelerators. Phys. Rev. ST Accel. Beams **14**, 010401 (2011). https://doi.org/10.1103/PhysRevSTAB.14.010401

40. P. Wang, H. Chen, J. Shi, et al., The RF design of a compact, high power pulse compressor with a flat output pulse, in Proc. 7th Int. Particle Accelerator Conf. (IPAC'16), Busan, Korea, paper THPMW022, pp. 3591–3593 May (2016)

41. P. Wang, H. Zha, I. Syratchev et al., rf design of a pulse compressor with correction cavity chain for klystron-based compact linear collider. Phys. Rev. Accel. Beams **20**, 112001 (2017). https://doi.org/10.1103/PhysRevAccelBeams.20.112001

42. Y. Jiang, H. Zha, P. Wang et al., Demonstration of a cavity-based pulse compression system for pulse shape correction. Phys. Rev. Accel. Beams **22**, 082001 (2019). https://doi.org/10.1103/PhysRevAccelBeams.22.082001

43. D. Wang, G. D'Auria, P. Delguisto, et al., Phase-modulation SLED mode on BTW sections at Elettra, in Proc. 23rd Particle Accelerator Conf. (PAC'09), Vancouver, Canada, paper TU5PFP099, pp. 1069–1071 May (2009)

44. Y. Jiang, J. Shi, P. Wang et al., The X-band pulse compressor for Tsinghua Thomson scattering X-ray source, in Proc. 8th Int. Particle Accelerator Conf. (IPAC'17), Copenhagen, Denmark, paper THPIK054, pp. 4214–4217 May (2017)